Nishimura *et al. Earth, Planets and Space* (2016) 68:144
DOI 10.1186/s40623-016-0517-y

Earth, Planets and Space

FULL PAPER

Open Access

Evolution of the current system during solar wind pressure pulses based on aurora and magnetometer observations

Yukitoshi Nishimura[1*], Takashi Kikuchi[2,3], Yusuke Ebihara[3], Akimasa Yoshikawa[4], Shun Imajo[4], Wen Li[1] and Hisashi Utada[5]

Abstract

We investigated evolution of ionospheric currents during sudden commencements using a ground magnetometer network in conjunction with an all-sky imager, which has the advantage of locating field-aligned currents much more accurately than ground magnetometers. Preliminary (PI) and main (MI) impulse currents showed two-cell patterns propagating antisunward, particularly during a southward interplanetary magnetic field (IMF). Although this overall pattern is consistent with the Araki (solar wind sources of magnetospheric ultra-low-frequency waves. Geophysical monograph series, vol 81. AGU, Washington, DC, pp 183–200, 1994. doi:10.1029/GM081p0183) model, we found several interesting features. The PI and MI currents in some events were highly asymmetric with respect to the noon–midnight meridian; the post-noon sector did not show any notable PI signal, but only had an MI starting earlier than the pre-noon MI. Not only equivalent currents but also aurora and equatorial magnetometer data supported the much weaker PI response. We suggest that interplanetary shocks impacting away from the subsolar point caused the asymmetric current pattern. Additionally, even when PI currents form in both pre- and post-noon sectors, they can initiate and disappear at different timings. The PI currents did not immediately disappear but coexisted with the MI currents for the first few minutes of the MI. During a southward IMF, the MI currents formed equatorward of a preexisting DP-2, indicating that the MI currents are a separate structure from a preexisting DP-2. In contrast, the MI currents under a northward IMF were essentially an intensification of a preexisting DP-2. The magnetometer and imager combination has been shown to be a powerful means for tracing evolution of ionospheric currents, and we showed various types of ionospheric responses under different upstream conditions.

Keywords: Sudden commencement, Solar wind dynamic pressure pulse, Field-aligned current, Dayside aurora

Introduction

Sudden commencements (SCs) are abrupt changes in the magnetic field that occur on a global scale and are caused by solar wind dynamic pressure jumps. Because of their distinct nature in magnetometer records, SCs have been used to study the response of the magnetosphere–ionosphere coupling system to solar wind disturbances. In addition to enhanced magnetopause currents that increase the low-latitude horizontal magnetic field (DL component, disturbance at lower latitudes), ionospheric currents and field-aligned currents (FACs) play an important role in characterizing ground magnetic field distributions (Nishida 1964; Tamao 1964; Araki 1994; Zesta et al. 2000; Chi et al. 2001; Kikuchi et al. 2001; Shinbori et al. 2009; Han et al. 2010). The main impulse (MI) of SCs is caused by two-cell ionospheric currents of the DP-2 (disturbance polar of the second type) type as well as a pair of region-1 (R1)-sense FACs. MIs are often preceded by a reversed sense of smaller magnetic field deflections called a preliminary impulse (PI), which corresponds to two-cell ionospheric currents of a reversed DP-2 type and a pair of R2-sense FACs. The initiation of both PI and MI magnetic field variations is considered

*Correspondence: toshi@atmos.ucla.edu
[1] Department of Atmospheric and Oceanic Sciences, University of California, Los Angeles, CA, USA
Full list of author information is available at the end of the article

to occur simultaneously across the entire latitude range including the magnetic equator, and this is attributed to rapid changes in large-scale electric fields (Boudouridis et al. 2011) and their instantaneous penetration to lower latitudes (Araki 1977; Kikuchi 1986). Recently, Kikuchi (2014) presented a comprehensive model of signal transmission from the magnetosphere to the equatorial ionosphere through the ionosphere–ground waveguide.

Global MHD simulations predict that an R2-sense FAC pair during the PI forms equatorward of preexisting DP-2 currents near noon and propagates azimuthally away from noon during its lifetime of a few minutes (Slinker et al. 1999; Fujita et al. 2003; Kim et al. 2009; Samsonov et al. 2010; Sun et al. 2015). An R1-sense FAC pair follows a similar sequence during the MI. The locations and propagation of the FACs provide useful information about the magnetospheric drivers, where the PI and MI currents are related to inertial currents of the compressional wave propagating through the magnetosphere and diamagnetic currents of tailward-propagating pressure structures behind the compressional wave, respectively. In addition, the interplanetary magnetic field (IMF) B_y, B_z, and Alfvén Mach number are known to alter FAC locations (Yu and Ridley 2011; Peng et al. 2011).

While ground magnetometers are widely used to study ionospheric currents during SCs, their evolution has been examined only in a limited number of studies (Araki et al. 1985; Stauning and Troshichev 2008; Han et al. 2010), and the predictions by global MHD simulations have not been tested comprehensively by observations. The current systems are often drawn using a few snapshots without addressing their propagation or PI–MI transition. Moreover, owing to the limited number of magnetometer stations, it has been difficult to show relative locations of currents prior to SCs and during PIs and MIs. Engebretson et al. (1999) reported an event showing dynamic evolution of equivalent ionospheric currents including a longitudinally propagating PI current by ~15°. Since magnetometers now cover a wide area on Earth, equivalent current motion can be traced over a larger spatial scale.

Another interesting behavior of the SC-related current system is that some SCs do not have a PI or show a PI only in a limited region. The peak occurrence probability of PIs at midlatitude is about 80 %, and the occurrence at low latitude is even lower (~50 %) (Araki et al. 1985; Yamada et al. 1997). Sastri et al. (2001) reported an event where a PI was not symmetric with respect to the noon meridian; the PI was detected only in the pre-noon sector. These studies indicate that PI currents do not always evolve in the conventional way described above, but that PI currents could be highly asymmetric or do not occur in some cases. By using equivalent current maps, we can determine how differently currents in such SCs evolve compared to currents during SCs with PIs in both pre- and post-noon sectors.

Although spatial resolution of ground magnetometers is not always sufficiently high to resolve relative locations of SC-related currents, this limitation can be mitigated by auroral measurements. Imaging from space and ground has demonstrated the capability of detecting auroral intensifications associated with solar wind dynamic pressure enhancements (e.g., Zhou and Tsurutani 1999; Boudouridis et al. 2003; Meurant et al. 2004; Liou et al. 2007; Holmes et al. 2014). A proton and electron diffuse aurora intensifies in the post-noon and pre-noon sectors and propagates antisunward. A discrete aurora poleward of diffuse aurora then intensifies in the post-noon sector. Motoba et al. (2009) and Liu et al. (2011) suggested that auroral behaviors are different during the PI and MI, potentially indicating that these differences can be used as an optical counterpart of SC-related FACs.

In the present study, we combine ground magnetometer and auroral observations to examine locations and propagation of preexisting DP-2, PI, and MI currents using four events for understanding evolution of SC-related currents. These four cases have different IMF and PI conditions: (1) a negative IMF B_z with a PI both pre- and post-noon, (2) a negative IMF B_z with a PI only pre-noon, (3) a positive IMF B_z with a PI both pre- and post-noon, and (4) a positive IMF B_z with a PI only pre-noon. We present and discuss similarities and differences in evolution of equivalent currents and auroral emissions.

Methods and dataset

SC events were identified as ΔSYM-H/Δt $\geq$ 5 nT/5 min associated with abrupt jumps in the solar wind dynamic pressure in ACE and WIND satellite data. PIs and MIs were found from ground magnetometer data in the high-latitude dayside sector as a bipolar change in the H-component (enhancement and then reduction pre-noon, and reduction and then enhancement post-noon, as shown in Fig. 1 and Additional file 1: Figure S1 for example). Equatorial magnetometer data were also used to assist with identifying PIs and MIs. Aurora data were obtained from the South Pole all-sky imager in Antarctica at −74.3° MLAT (Ebihara et al. 2007). We required that the South Pole imager was located between 12- and 16-h MLT under favorable sky conditions in southern polar nights. Imager data in the green (557.7 nm) and red (630.0 nm) wavelengths were projected onto the 110- and 250-km altitude planes, respectively. The 630.0-nm aurora is sensitive to low-energy (less than ~1 keV) electron precipitation, whereas the 557.7-nm aurora responds to high-energy (greater than ~1 keV) electron and proton precipitation through secondary electrons. The time resolution varies between 9 and 44 s.

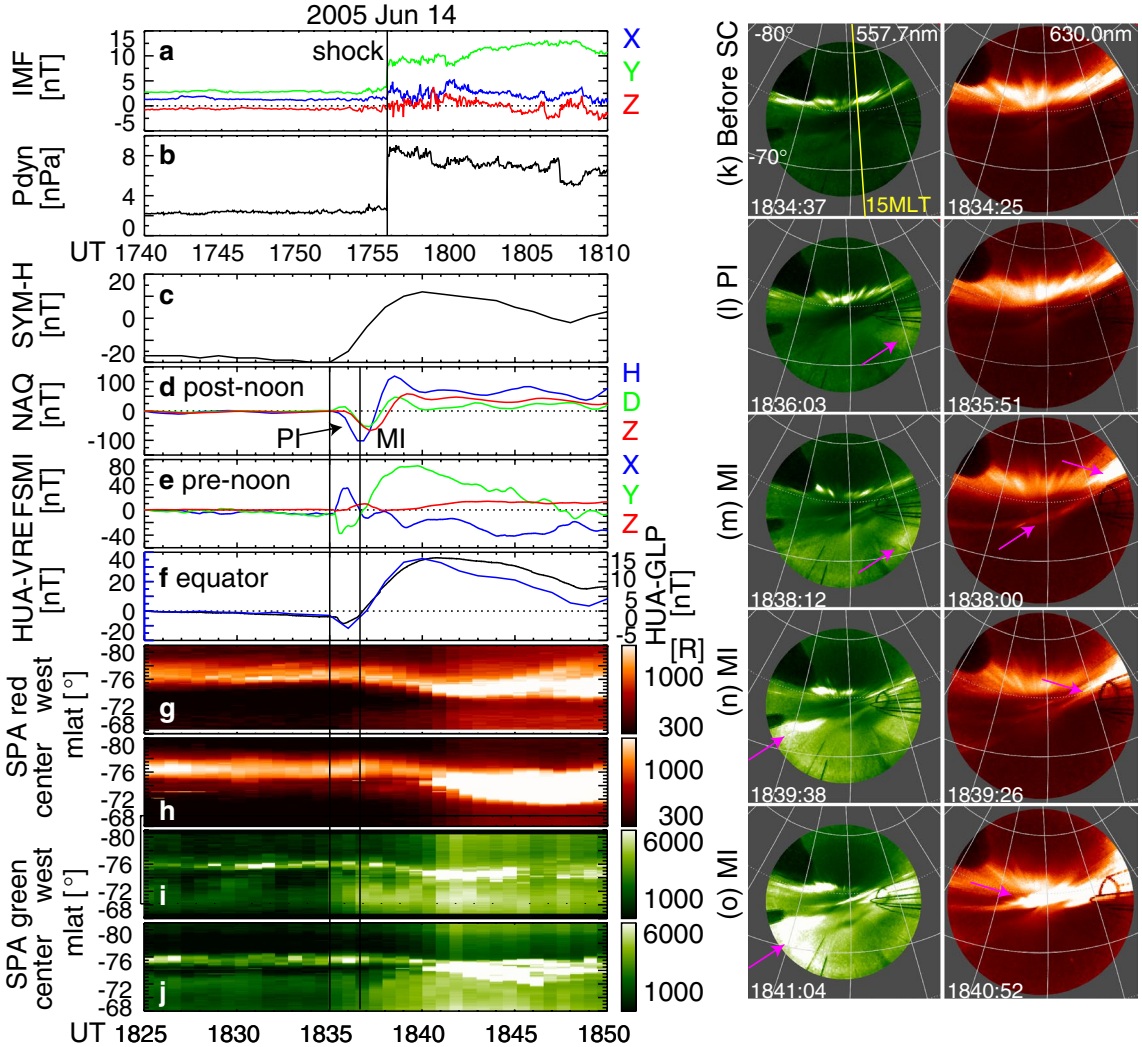

Fig. 1 Magnetic field and auroral sequence of the June 14, 2005, SC event. **a** IMF in GSM; **b** solar wind dynamic pressure at WIND; **c** SYM-H; magnetometer data at **d** Narsarsuaq [65.88° MLAT, ~17 MLT, in altitude adjusted corrected geomagnetic (AACGM)] and **e** Fort Smith (67.44° MLAT, ~10.3 MLT); **f** 1-min resolution H-component data (*blue*) from Huancayo (0.62° MLAT, ~15 MLT) relative to Villa Remedios (−4.89° MLAT, ~15 MLT) together with 1-s data (*black*) from Huancayo relative to Guadalupe (−2.8° MLAT, ~15 MLT); *red line* keograms in the **g** western and **h** central portion of the South Pole imager FOV; and *green line* keograms in the **i** western and **j** central portion of the imager FOV. **k**–**o** Selected snapshots of the (*left*) *green* and (*right*) *red line* data. The *pink arrows* highlight the major auroral brightenings during the PI and MI. The South Pole station was on the post-noon sector near 15-h MLT. The *vertical line* in **a**, **b** marks the dynamic pressure jump. The first and second *vertical lines* in panels **c**–**j** are the PI and MI onset times in the post-noon sector

The Time History of Events and Macroscale Interactions during Substorms (THEMIS) (Russell et al. 2008) and SuperMAG (Gjerloev 2012) magnetometer data in the Northern Hemisphere were used to obtain 2-D equivalent current patterns (in a 1-min cadence) by rotating horizontal magnetic field perturbations by 90° clockwise when viewing from above. Data just before the onset of SCs were used to subtract baselines (the time used for a baseline is indicated in figure captions). To remove magnetopause current effects (DL component), the H-component variations at the dayside low latitude at San Juan multiplied by the cosine of each station latitude divided by the cosine of the San Juan latitude (29.1° in AACGM) were subtracted from the H-component data of each station at each time. Because of the northern daylight conditions in our events (between late April and July), it is reasonable to assume that the ionospheric conductance in the dayside polar ionosphere is high and its spatial gradients are small. Under such conditions, equivalent currents have been widely used as an indicator

of ionospheric Hall currents (e.g., Richmond and Kamide 1988), and effects of FACs are limited to ~10 % of magnetic field perturbations (Sun et al. 1985). In this condition, the electric field associated with a clockwise Hall current cell should point away from the center of the current cell. Pedersen currents flow parallel to the electric field and thus connect to downward FACs at the center of the Hall current cell. Similarly, upward FACs are inferred at the center of a counterclockwise Hall current cell. When upward FACs are located near the imager, they are expected to correspond to auroral brightenings in both the red and green lines, as those are carried by precipitating electrons. Downward FACs may correspond to a diffuse auroral brightening in the green line if sufficient proton precipitation occurs. Such a relation can validate the accuracy of equivalent current maps because auroral imaging can specify FAC locations at a much higher spatial resolution even though the spatial coverage is limited. The use of ground magnetometers has an advantage compared to satellite-based magnetic field measurements because of fast temporal variations in SC-related currents. Nevertheless, we validated FAC locations for the first event using Defense Meteorological Satellite Program (DMSP) data (Hardy et al. 1984; Rich 1984) to assist with the interpretation of the auroral signatures. We also referred to Active Magnetosphere and Planetary Electrodynamics Response Experiment (AMPERE) data for the second event. Equatorial magnetometer data from the Magnetic Data Acquisition System/Circum-pan Pacific Magnetometer Network (MAGDAS/CPMN, 1 s) (Yumoto and the MAGDAS Group, 2006) and SuperMAG (1 min) were also used to find effects of penetration electric fields.

Results

Event 1 (southward IMF with post-noon PI)

The event in Fig. 1 has a large SYM-H amplitude of 42 nT associated with a solar wind dynamic pressure pulse preceded by a steady SYM-H level (Fig. 1b, c). This interplanetary shock was measured by both WIND and ACE and was the only shock event around this time (see Additional file 1: Figure S1 for details). Thus, this is an isolated SC event. The IMF was directed slightly southward before the shock (with large B_y, Fig. 1a) and then became almost zero for the first few minutes after the shock at WIND, while IMF B_z remained negative at ACE. The onset times of the PI and MI can be identified from the 1-s resolution of the magnetometer data in the post-noon polar region (Fig. 1d) as 1835:10 and 1836:50 UT as an abrupt drop and rise in the H-component. However, the PI in the pre-noon sector was initiated slightly later at 1836:09 UT, and the duration of the PI was ~1 min shorter (Fig. 1e). This is not because of the choice of stations but can also be seen in the equivalent currents below. The meridional chains of the magnetometer data pre- and post-noon shown in Additional file 1: Figure S1 confirm the differences in the PI onset time and duration. The equatorial magnetometer data in the post-noon sector show a typical PI and MI (Fig. 1f), and the ratio of the PI and MI amplitudes relative to the level just before the SC (~−5 nT) was 0.23. Here, differences in the magnetic fields between Huancayo (0.62° MLAT) and Villa Remedios (−4.89° MLAT) are used to extract dayside equatorial ionospheric effects since both stations see essentially the same magnetospheric current effects but equatorial electrojet effects are confined within a few degrees from the magnetic equator (Kikuchi et al. 2001).

The aurora data of this event have been presented by Motoba et al. (2009), and we use this as a reference event. The South Pole station was located near 15-h MLT. Figure 1g–j shows geomagnetic north–south keograms of the South Pole imager data for the 630.0- and 557.7-nm wavelengths in the central and western portions of the imager field of view (FOV). Two-dimensional snapshots at five instances are displayed in the right columns. Prior to the SC, a steady discrete auroral arc and a faint diffuse auroral band were present at ~−76° and −72° MLAT, respectively. The diffuse aurora equatorward of −75° MLAT for the 557.7-nm wavelength suddenly brightened during the PI (Fig. 1l, highlighted by the pink arrow), whereas the discrete aurora for both wavelengths did not show any notable change. This brightening was seen more predominantly near the western edge of the imager FOV, i.e., close to magnetic noon. Then, the diffuse auroral brightness further increased during the MI and was later also seen in the eastern portion of the imager FOV. The discrete aurora for the 630.0-nm wavelength also brightened during the MI phase in the western portion of the imager FOV (Fig. 1m, right), and this brightening was connected to a new faint arc that formed equatorward of the preexisting discrete auroral arc. The brightening extended to the east along the newly formed equatorward arc (Fig. 1k, right), and the new equatorward arc then became the dominant auroral structure after the poleward arc merged with the equatorward arc (Fig. 1o, right).

The DMSP satellites passed the duskside polar region before and after the onset of the SC. Since the satellites passed a few-hour MLT away from the imager in the Northern Hemisphere, the latitudes of precipitation and FACs in Fig. 2 are not expected to match the auroral signatures in Fig. 1, but we can qualitatively compare the overall patterns of the magnetic field and particle precipitation to the latitudinal auroral distributions. The east–west magnetic field amplitude was ~100–200 nT before the SC and then increased to ~320 nT after the onset of

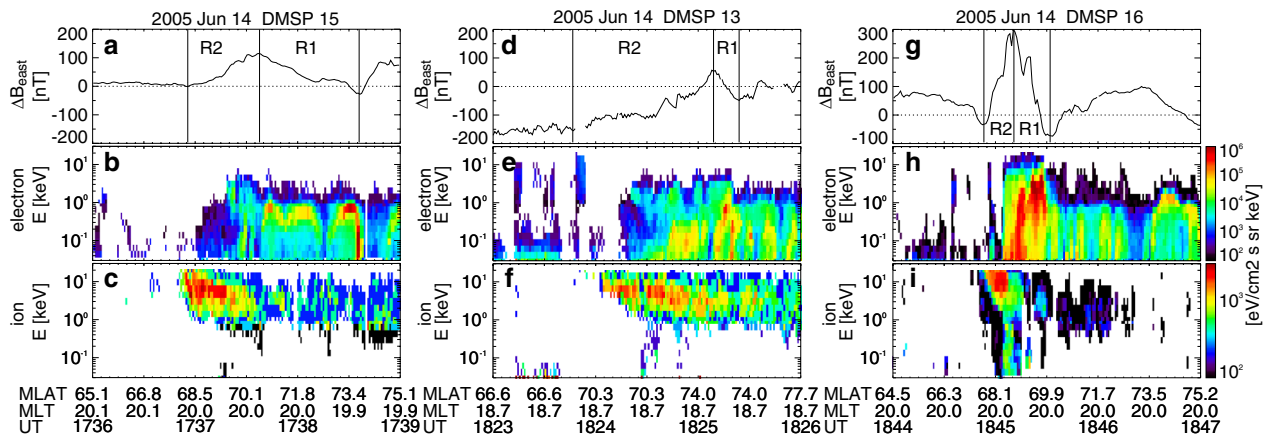

Fig. 2 DMSP data (*left* and *middle*) before and (*right*) after the shock arrival in Fig. 1. **a**, **d**, **g** Cross-track magnetic field deviation (positive eastward), **b**, **e**, **h** electron energy flux, and **c**, **f**, **i** ion energy flux. The *vertical lines* mark the changes in the large-scale magnetic field slopes

the SC during the enhanced auroral intensity in the MI phase. The enhanced electron precipitation likely corresponds to the discrete auroral intensification shown in Fig. 1, and this was associated with the upward R1 FAC. While the electron fluxes equatorward of the R1 FAC remained weak, the ion precipitation fluxes within the downward R2 FAC (~68 MLAT) increased substantially. Thus, the diffuse auroral intensification would be caused by enhanced ion precipitation in the downward R2 FAC. This interpretation is consistent with global imaging (Zhang et al. 2008; Motoba et al. 2009; Holmes et al. 2014) and particle observations (Egeland et al. 1994; Zhou et al. 2003).

Figure 3 shows the equivalent current patterns from the magnetometer data in the dayside Northern Hemisphere. The current pattern before the SC (Fig. 3a) was obtained by taking differences in the magnetic fields between 1834 UT and the initiation of a DP-2 enhancement at 1820 UT. A clockwise current was seen in the pre-noon sector, as visually traced by the pink line, while a counterclockwise current was seen in the post-noon sector. These two currents are consistent with a typical DP-2 current pattern under two-cell convection. An R1 sense of the FACs can be inferred, as marked by the upward and downward arrows, and the inferred upward FAC latitude (~75°–80°) is roughly consistent with the preexisting discrete aurora at −76° MLAT in the imager data, although they are simply for illustration and likely have uncertainties due to the limited number of observation points and unknown electric field and conductance profiles.

Figure 3b–h shows the equivalent current patterns during the PI and MI phases using the magnetic field deviations from those just before the SC at 1834 UT. During the PI phase, a counterclockwise current cell formed in the pre-noon sector, indicating an upward FAC (Fig. 3b), although no substantial perturbations were seen in the post-noon sector within the available magnetometers (see also Fig. 1d, e). This current formed slightly equatorward and sunward of the preexisting DP-2 currents. The counterclockwise current cell amplified and moved antisunward by ~3-h MLT in 1 min (Fig. 3c), and the post-noon stations detected a clockwise current cell, indicating a downward FAC. The inferred downward FAC is located near the center of the northern conjugate of the South Pole imager FOV, where diffuse auroral intensification is shown in Fig. 1g and h. This current cell also propagated by ~3-h MLT in 3 min and survived longer than the pre-noon PI current cell.

Another pair of DP-2-sense currents formed closer to noon in Fig. 3d, e, and they can be considered as the MI current system. Similar to the PI current system, the current intensity was asymmetric with a larger current cell in the pre-noon sector. In the post-noon sector, the preexisting PI current cell still existed and continued propagating antisunward with a decreasing intensity. The MI currents further intensified and also propagated antisunward (Fig. 3e–h). The antisunward motion of the upward FAC in the MI current system occurred at about the same latitude and timing of the 630.0-nm auroral propagation in Fig. 1k–m, suggesting that the 630.0-nm aurora highlights the evolution of the upward FAC portion of the MI current system.

To summarize this event, the PI and MI current patterns can be characterized by two pairs of current cells that form near noon and then propagate antisunward. Although the PI currents were asymmetric in terms of timing, the behaviors were similar. On the basis of the timing and location, the diffuse auroral intensification

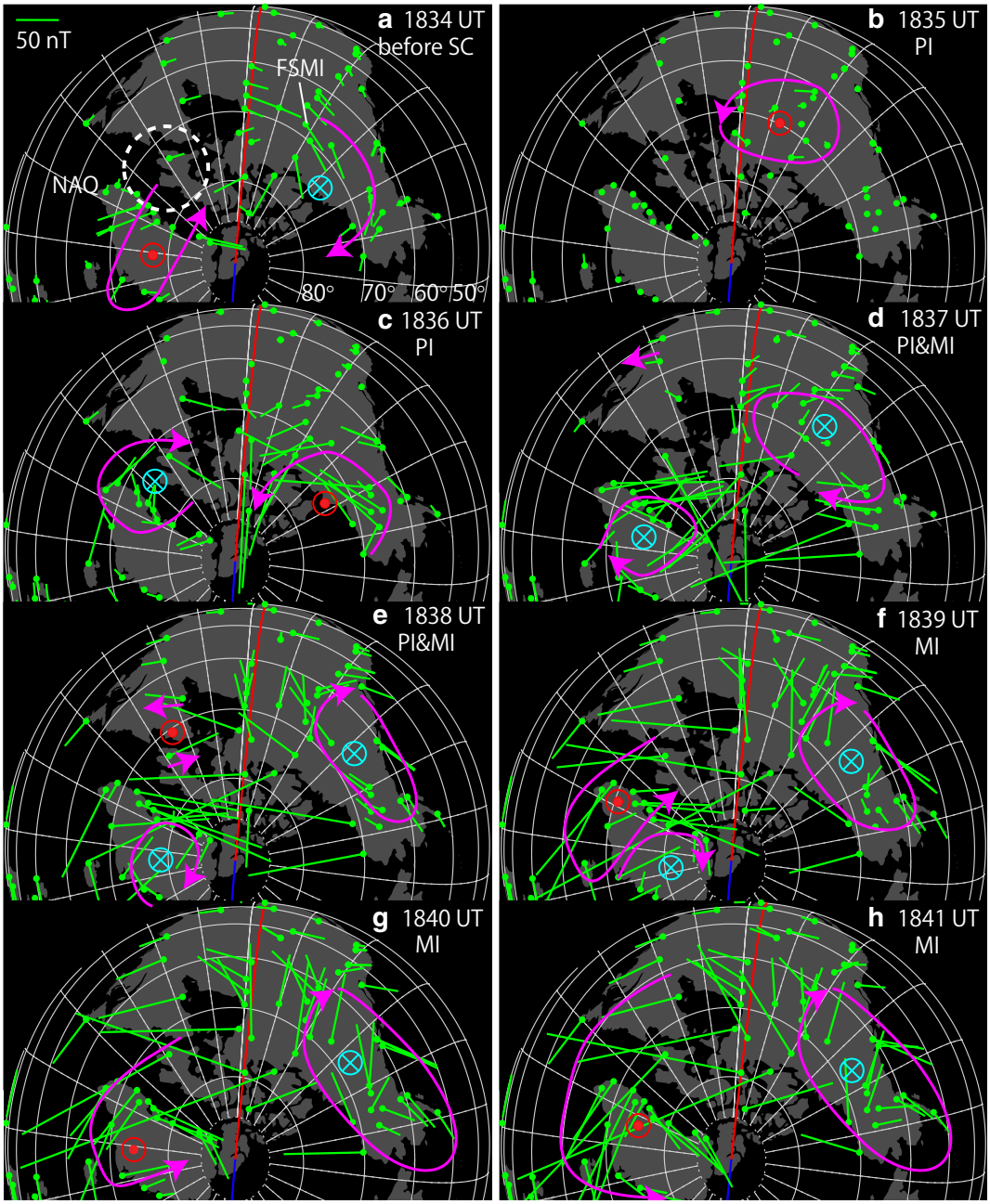

Fig. 3 Equivalent current vectors during the event in Fig. 1. **a** Magnetic field before the onset of the PI using 1820 UT as the baseline. The *white circle* in **a** shows the South Pole imager FOV mapped to the Northern Hemisphere using IGRF. **b**–**h** Magnetic fields during the PI and MI using 1834 UT as the baseline. The *pink lines* visually trace the representative current vectors, and the upward and downward arrows schematically illustrate the upward and downward FACs. The magnetic noon and midnight meridians are marked by the *red* and *blue lines*, respectively

during the PI phase can be related to the post-noon downward FACs associated with the PI clockwise equivalent current. Since the diffuse aurora is latitudinally separated from the discrete aurora, the PI current can be seen as a separate current system from the preexisting DP-2 and would be mapped to the dayside magnetosphere on closed magnetic field lines. The upward FAC portion of the MI current system can be represented by the discrete auroral brightening. This has the same sense as the preexisting DP-2 and occurs along the same discrete arc. However, this is a separate current system that forms close to noon and then develops equatorward of the preexisting

DP-2 as the currents propagate antisunward, becoming post-SC DP-2 currents. Although the equivalent currents have limitations, as mentioned in the previous section, their use in combination with the imager data allows for the identification of the detailed evolution of the FACs observationally.

Although it is difficult to quantitatively determine the magnetic field mapping accuracy for a dynamically evolving magnetic field geometry during shocks according to our prior work (Nishimura et al. 2013), the accuracy of the model magnetic field mapping is a few degrees in latitude and ~1-h MLT. Since the 630.0-nm auroral arcs spread over ~3° in latitude and elongate in the east–west direction, these model uncertainties would fall within the extent of the large-scale FACs shown in the equivalent current maps. In fact, we showed that the mapped auroral location is within the equivalent current cells.

Event 2 (southward IMF without post-noon PI)

The SC of the event in Fig. 4 has a similarly large amplitude (50 nT in SYM-H) to event 1 under a southward IMF associated with a dynamic pressure jump. A major difference from the previous event is that the post-noon high-latitude magnetometer (Fig. 4d) did not show any signs of a PI, although a PI can be seen clearly in the magnetometer data at the pre-noon high-latitude and post-noon equator starting at 1810 UT (Fig. 4e, f), indicating that the post-noon high-latitude PI was much shorter than the 1-min resolution of the data or not present. Instead, the H-component showed a gradual rise that started at 1809 UT or earlier, even though the interplanetary shock front was as sharp as in the previous event. The magnetometers at other latitudes in the post-noon sector also did not detect any PI signature (Additional file 2: Figure S2). The PI and MI onset times were identified from the pre-noon magnetometer data as 1809:56 and 1810:51 UT. Although the equatorial magnetometer data show a PI, the ratio of the PI and MI amplitudes (0.12) was about half of that in event 1, indicating that penetration to the equator was not as efficient as in event 1.

The discrete aurora for the 630.0-nm wavelength abruptly brightened at the onset of the MI, and the center of activity shifted equatorward in a similar manner to the previous event (Fig. 4g, k–o). During the MI, the preexisting arc slowly faded away, and the equatorward arc became the dominant structure (Fig. 4h, k–m), indicating that the MI current system is a separate structure from the preexisting DP-2. On the other hand, the 557.7-nm diffuse auroral intensity slowly increased only during the PI and then abruptly intensified at the onset of the MI (Fig. 4i–m). The lack of clear magnetic and auroral signatures of the PI indicates that the post-noon PI current was not present or much smaller than that in event 1. If we do not have auroral measurements, we cannot rule out the possibility that the lack of a PI in the magnetometer data might be because the PI signal was masked by an MI signal or occurred far away from noon. However, the smaller diffuse auroral luminosity indicates that the PI signal in the post-noon sector was indeed substantially smaller than that in event 1.

The lack of a post-noon PI can be confirmed in the equivalent current patterns shown in Fig. 5. DP-2 currents existed prior to the SC, with a westward electrojet around the latitude of the discrete aurora within the imager FOV. Enhanced DP-2-type two-cell currents—hence MI currents—were the dominant structures throughout the SC, and the only noticeable signature of the PI is a small counterclockwise current cell in the pre-noon sector (Fig. 5c). This may be a downward extension of the post-noon counterclockwise cell. The center of the post-noon MI currents was found at ~73° MLAT, consistent with the location of the 630.0-nm emission in Fig. 4g, h. Although it is difficult to find a difference between the latitudes of the preexisting and MI currents, the auroral observations suggest that the MI currents formed slightly equatorward of the preexisting DP-2. The FAC locations before and after the SC are roughly consistent with the major FACs in the AMPERE data (Additional file 3: Figure S3), although AMPERE also shows much more structured FAC patterns.

The difference in the PI current evolution of these two events raises the question of why the PI currents in event 2 were much smaller and asymmetric than those in event 1, even though they are both comparably large SC events caused by ~8-nPa jumps in the solar wind dynamic pressure. We noticed a difference in the shock normal orientation relative to the Sun–Earth line based on the shock arrival timing at WIND and ACE, and the role of the shock angle is discussed in "Shock orientation" section. Although the IMF B_y may also contribute to the asymmetric responses, the PI currents in events 1 and 2 are quite different, even though the magnitude of the IMF B_y behind the shocks is only different by a factor of ~2. The MI currents in event 1 became asymmetric (Fig. 3h), but the MI currents in event 2 were more symmetric (Fig. 5f). From these comparisons, we do not see an indication that the IMF B_y contributes to the asymmetric response mentioned above.

Event 3 (northward IMF with post-noon PI)

Figure 6 shows an SC event with a 13-nT increase in SYM-H during a northward IMF associated with a dynamic pressure jump. WIND was located in the solar wind downstream of Earth (Additional file 4: Figure S4). A PI and an MI were seen in both pre- and post-noon sectors simultaneously as well as at the equator. The PI

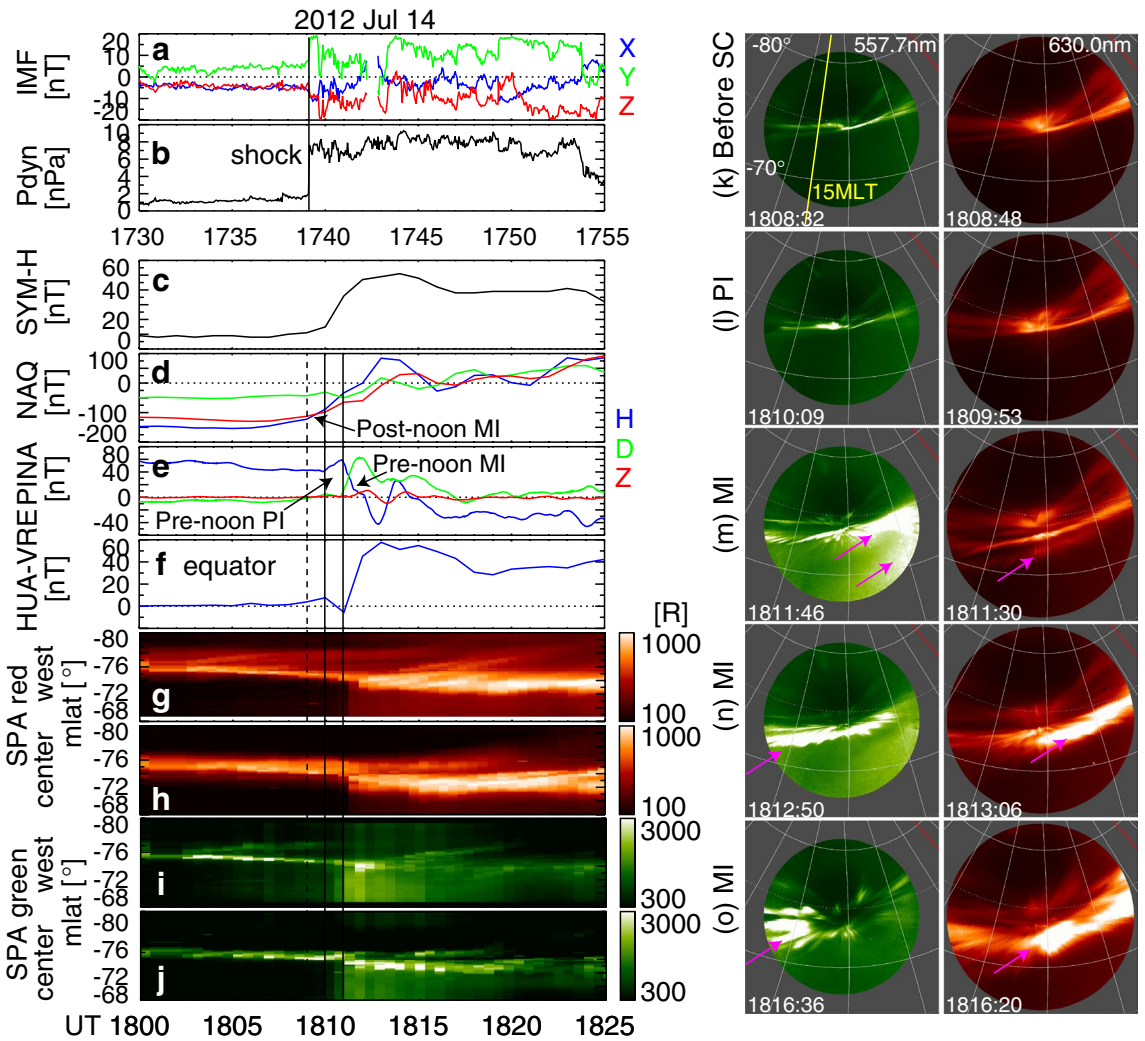

Fig. 4 Same as Fig. 1 but for the July 14, 2012, SC event without post-noon PI. The magnetometer in **e** is at Pinawa (60.22° MLAT, ~11.5 MLT)

and MI onset times were at 1602:32 and 1605:04 UT, respectively (see also Additional file 4: Figure S5).

The 557.7-nm diffuse aurora started to brighten during the PI phase equatorward of the preexisting 630.0-nm auroral arc and reached almost the maximum intensity level before the MI (Fig. 6i–l). The 630.0-nm auroral arc brightening occurred during the MI (Fig. 6g, h, k, m). In contrast to events 1 and 2, the arc did not substantially move equatorward but remained essentially at the same latitude. These wavelength-dependent intensifications again indicate that high-energy (seen for 557.7 nm) and low-energy (for 630.0 nm) precipitations have different roles in carrying currents. The diffuse aurora is likely an indicator of the PI currents, which occurred ~8° equatorward of the preexisting currents in this case. The MI currents appear to be an intensification of preexisting currents.

The equivalent current pattern prior to the SC showed a DP-2-type pattern (Fig. 7a). A current pair with an opposite sense formed during the PI phase (Fig. 7b) and remained for ~3 min at ~1- to 2-h MLT of the antisunward propagation (Fig. 7c, d). Duskside MI currents started to form in Fig. 7c much more equatorward of the PI currents, and pre-noon MI then appeared 1 min later in Fig. 7d. The PI and MI currents coexisted until the MI currents became a dominant signature.

Event 4 (northward IMF without post-noon PI)

The SC event in Fig. 8 had a similar (15 nT) amplitude in SYM-H to that in event 3 under a northward IMF. In the pre-noon sector, the PI and MI were initiated at 1624:13 and 1627:00 UT (Fig. 8e). On the other hand, no PI signature was seen in the post-noon sector, but an increase in the MI-type H-component occurred 1 min earlier

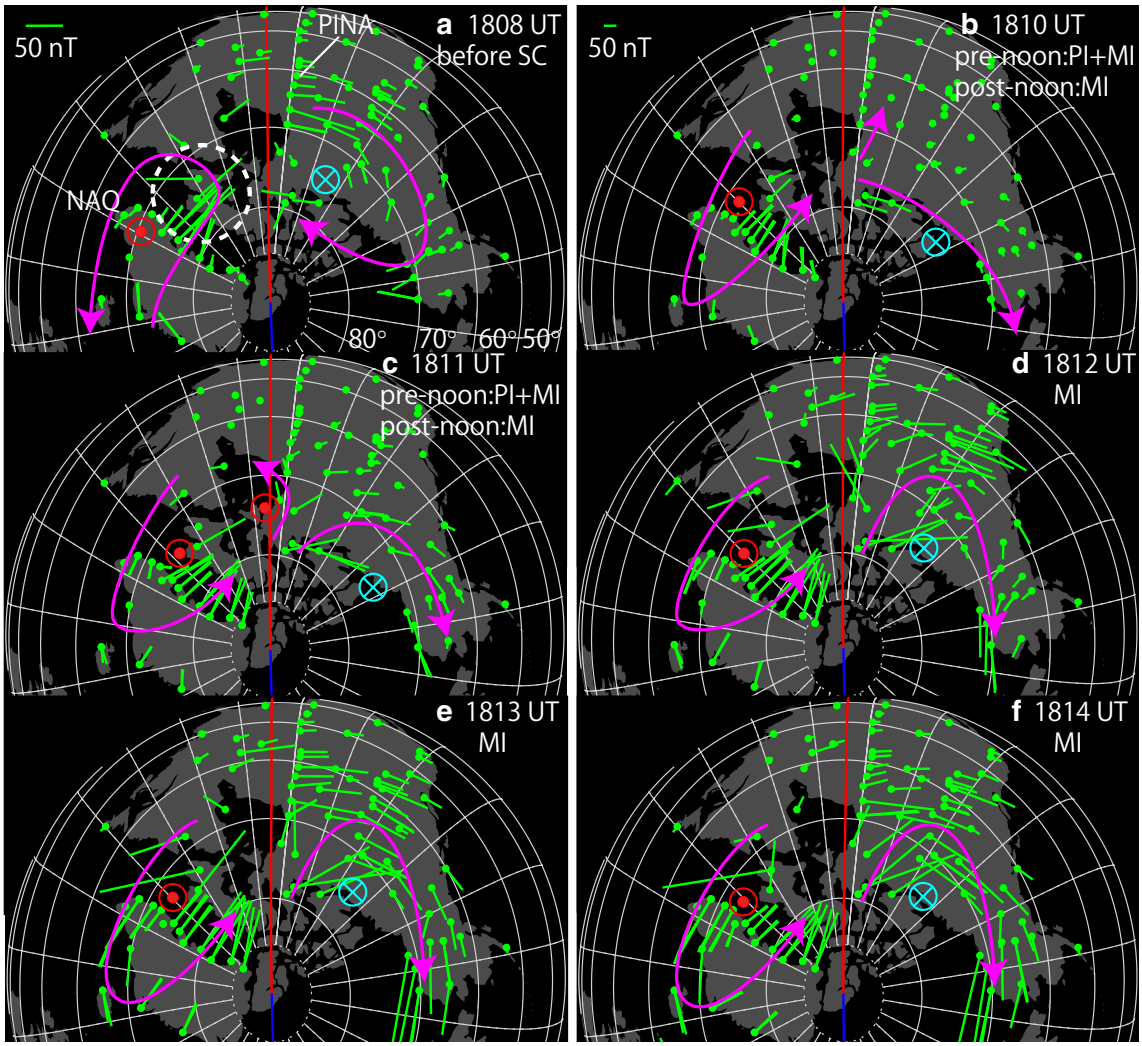

Fig. 5 Same as Fig. 3 but for the July 14, 2012, SC event with 1800 UT as the baseline of **a**

(Fig. 8d, see also Additional file 5: Figure S5). The equatorial magnetometer data in Fig. 8f also did not show any PI signature, but a gradual rise started earlier than the onset of the SC in Fig. 8e.

Unlike the previous events, the discrete aurora at ~75° MLAT for both 557.7 and 630.0 nm started to brighten during the PI and then intensified further during the MI with a small equatorward expansion. This may be related to the early initiation of the post-noon MI. The 557.7-nm diffuse aurora was negligibly weak during the PI but abruptly intensified during the MI. The lack of diffuse auroral brightening during the PI suggests that the PI current in the post-noon sector was very weak and that the MI current dominated the post-noon current system throughout the SC, even though the pre-noon sector had both a PI and an MI.

An asymmetric current system can also be seen in the equivalent current distribution in Fig. 9. In the pre-noon sector, a counterclockwise PI current cell formed at ~8 MLT and then stretched antisunward (Fig. 9b, c) before the MI currents became a dominant structure (Fig. 9d). In contrast, there is no notable signature of a PI in the post-noon sector, but the post-noon current pattern is dominated by a counterclockwise MI current cell.

Although the SCs in events 3 and 4 are both driven by solar wind dynamic pressure jumps of ~2 nPa under a northward IMF, the PI aurora and currents have striking differences. We discuss a possible cause of this in "Shock orientation" section. The IMF B_y is negative in events 3 and 4. Although $|B_y|$ is larger in event 3 (~10 nT) than in event 4 (<5 nT), the PI currents are more symmetric in event 3. The MI currents are symmetric in both cases. In

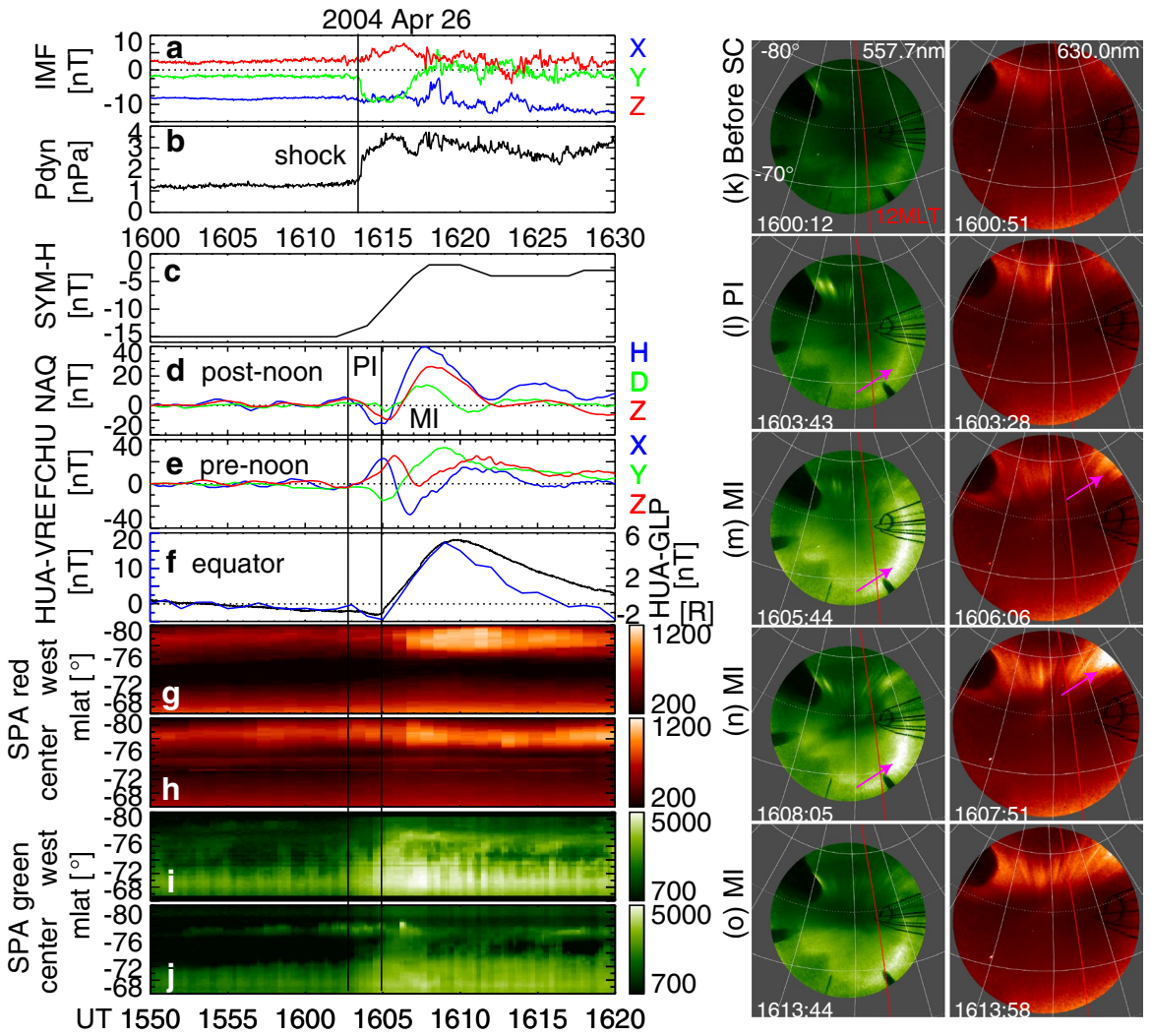

Fig. 6 Same as Fig. 1 but for the April 26, 2004, SC event under a northward IMF. The magnetometer in **e** is at Fort Churchill (68.65° MLAT, ~9.4 MLT). Note that WIND in this event was located in the downstream of Earth

these comparisons, we do not see a consistent pattern of IMF B_y effects.

Shock orientation

In "Event 1 (southward IMF with post-noon PI)", "Event 2 (southward IMF without post-noon PI)", "Event 3 (northward IMF with post-noon PI)", and "Event 4 (northward IMF without post-noon PI)" sections, we showed that PI currents can be highly asymmetric and sometimes undetectably small within the dayside magnetometer coverage, even though these events are all associated with sharp solar wind dynamic pressure jumps. Sastri et al. (2001) also reported an asymmetric PI current pattern and speculated that shock impacts away from the Sun–Earth line could induce asymmetric PI currents. To test this hypothesis, we calculated the shock normal using the ACE and WIND measurements shown in the figures in Additional file 1: Figure S1, Additional file 2: Figure S2 and Additional file 4: Figure S4, Additional file 5: Figure S5. Takeuchi et al. (2002) compared different methods for calculating a shock normal and showed that a time lag method gives the most reasonable solution. In this method, assuming that the shock normal is located on the ecliptic plane and the shock propagates with a constant solar wind speed behind the shock, the time lag of the shock measurements at two different locations in the solar wind gives the orientation. Although the shock normal could also have a component out of the ecliptic plane, it does not explain the asymmetry with respect to the noon–midnight meridian and thus is not considered in this study.

Table 1 lists the results of the normal-angle calculation. In events with the PI in both pre- and post-noon

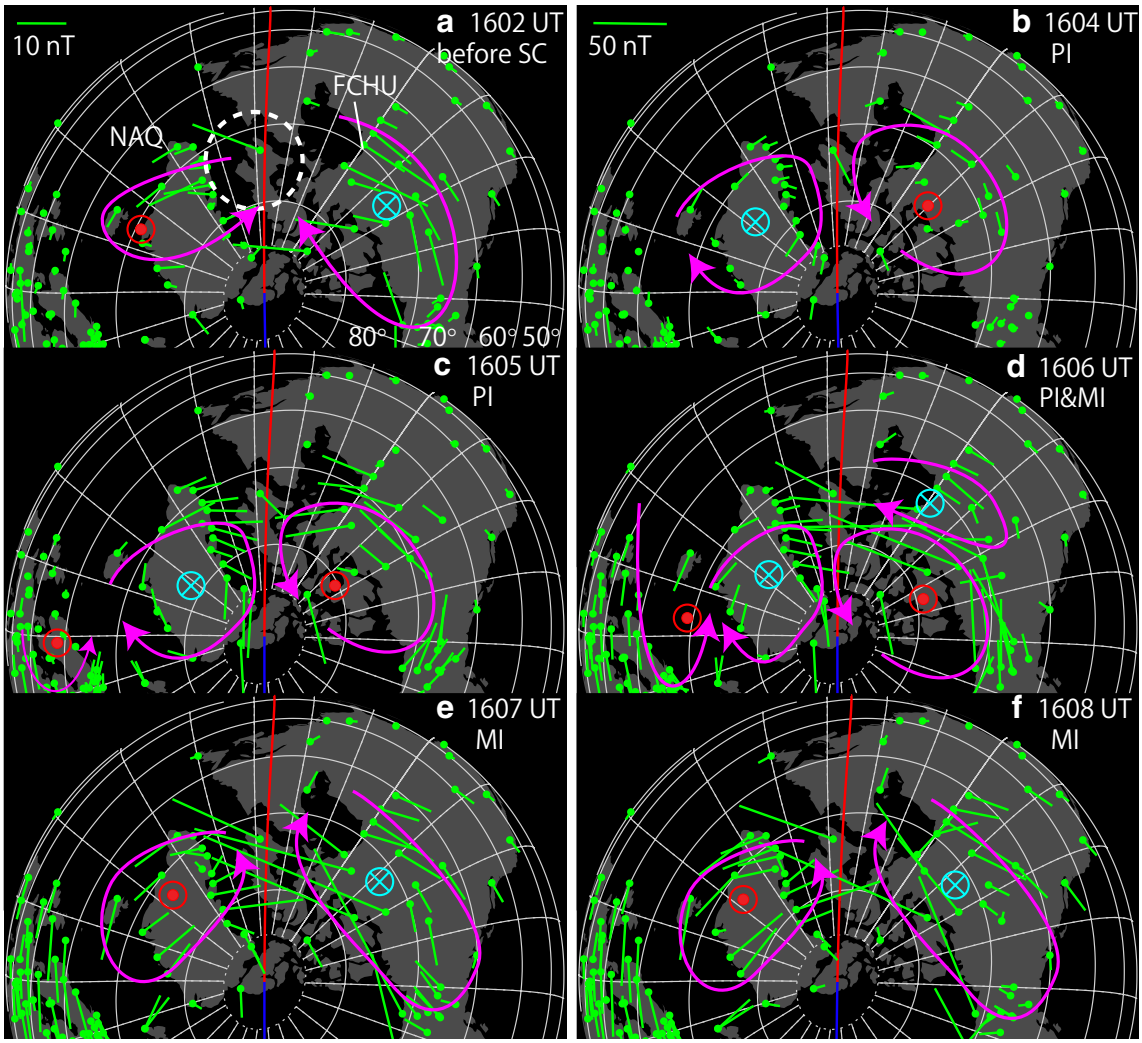

Fig. 7 Same as Fig. 3 but for the April 26, 2004, SC event with 1600 UT as the baseline of **a**

sectors (events 1 and 3), the shock normals were tilted by only 4° and 7° toward dusk from the Sun–Earth line. This explains the roughly symmetric PI and MI currents in the pre- and post-noon sectors. In contrast, the shock normals of events 2 and 4 are more tilted from the Sun–Earth line (12° and 14° toward dawn). This means that the shocks impact the magnetopause away from the subsolar point toward dusk (the contact point to the bow shock for a 14° tilt shock is $Y \sim 7R_E$) and that the shocks compress the magnetosphere more gradually (Takeuchi et al. 2002). The gradual compression from dusk explains the gradual development of the MI in the post-noon sector prior to the MI initiation in the pre-noon sector. The lack of a post-noon PI would be because the MI signal reached the ionosphere earlier than the PI current system developed under gradual compression or because the post-noon PI shifted nightside and became difficult to detect owing to low conductance.

For a comparison, we also estimated the normal angles using the minimum variance analysis (MVA) and coplanarity methods (Takeuchi et al. 2002; Keika et al. 2009). Data within a 5-min window around each shock were used for the MVA, and 1-min median-filtered data before and after each shock were used for the coplanarity method. The azimuthal normal angles estimated by the MVA are close those from the time lag method. The longitudinal angles are not zero but are confined within 30°. However, note that unlike the discontinuities studied by Keika et al. the med/min eigenvalue ratio is <3. As shown in Additional file 1: Figure S1, Additional file 2: Figure S2 and Additional file 4: Figure S4, Additional file 5: Figure S5, the magnetic field jumps across the shocks are often

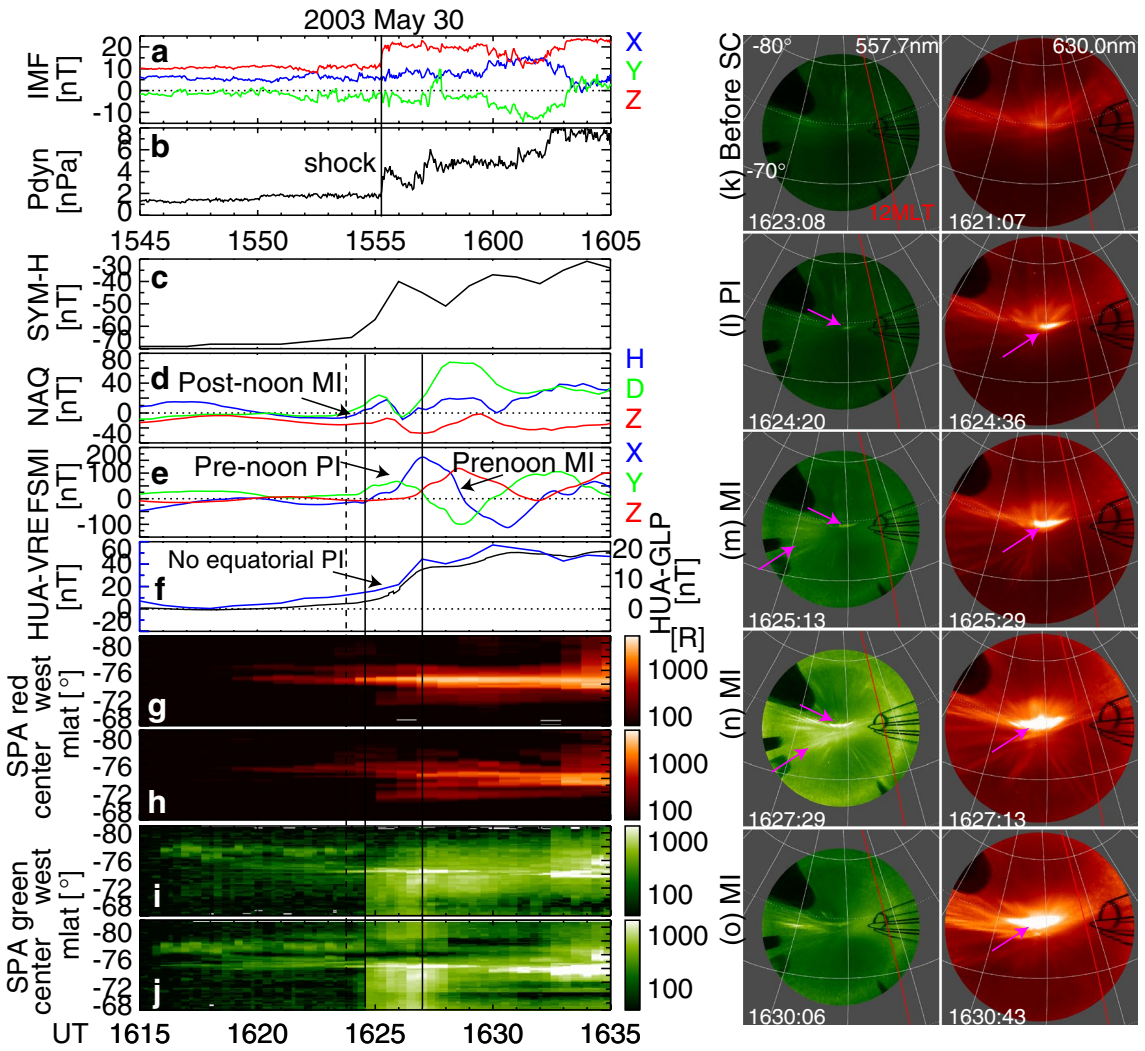

Fig. 8 Same as Fig. 1 but for the May 30, 2003, SC event under a northward IMF without a post-noon PI. FCHU is located at ~9.7 MLT

linearly polarized in the GSM Y or Z directions; thus, the median and minimum variance directions are not determined precisely. This may explain ~10° differences between the time lag and MVA methods. The azimuthal angles estimated using the coplanarity method are quite different from the other two methods. Such a difference was also seen in the analysis of Takeuchi et al., and the quasi-linear polarization nature of the changes in the magnetic field at the shocks may again introduce large uncertainties in the coplanarity method.

According to Araki et al. (2004) and Wang et al. (2006), a larger shock normal angle from the Sun–Earth line leads to a more gradual SC because the shock sweeping time across a geoeffective length [30 R_E by Araki et al. (2004)] becomes longer. However, the SYM-H rise time in our events does not show a clear dependence on the shock normal angle (Table 1). According to Fig. 3 of Wang et al. (2006), a substantial increase in the rise time seems to occur for events with a normal angle of less than ~150°. Thus, the lack of a rise-time normal-angle dependence in our events could be because of the small normal angles from the Sun–Earth line. Our results indicate that even small shock normal angles from the Sun–Earth line can drive asymmetric responses in the PI and MI currents.

Conclusion

By combining aurora and magnetometer data, we observationally identified evolution of the currents during four isolated SC events. The large amount of magnetometer data allowed us to trace evolution of the PI and MI equivalent currents. The PI current pair formed equatorward and sunward of the preexisting DP-2 currents, and in event 1 with a southward IMF, it propagated antisunward

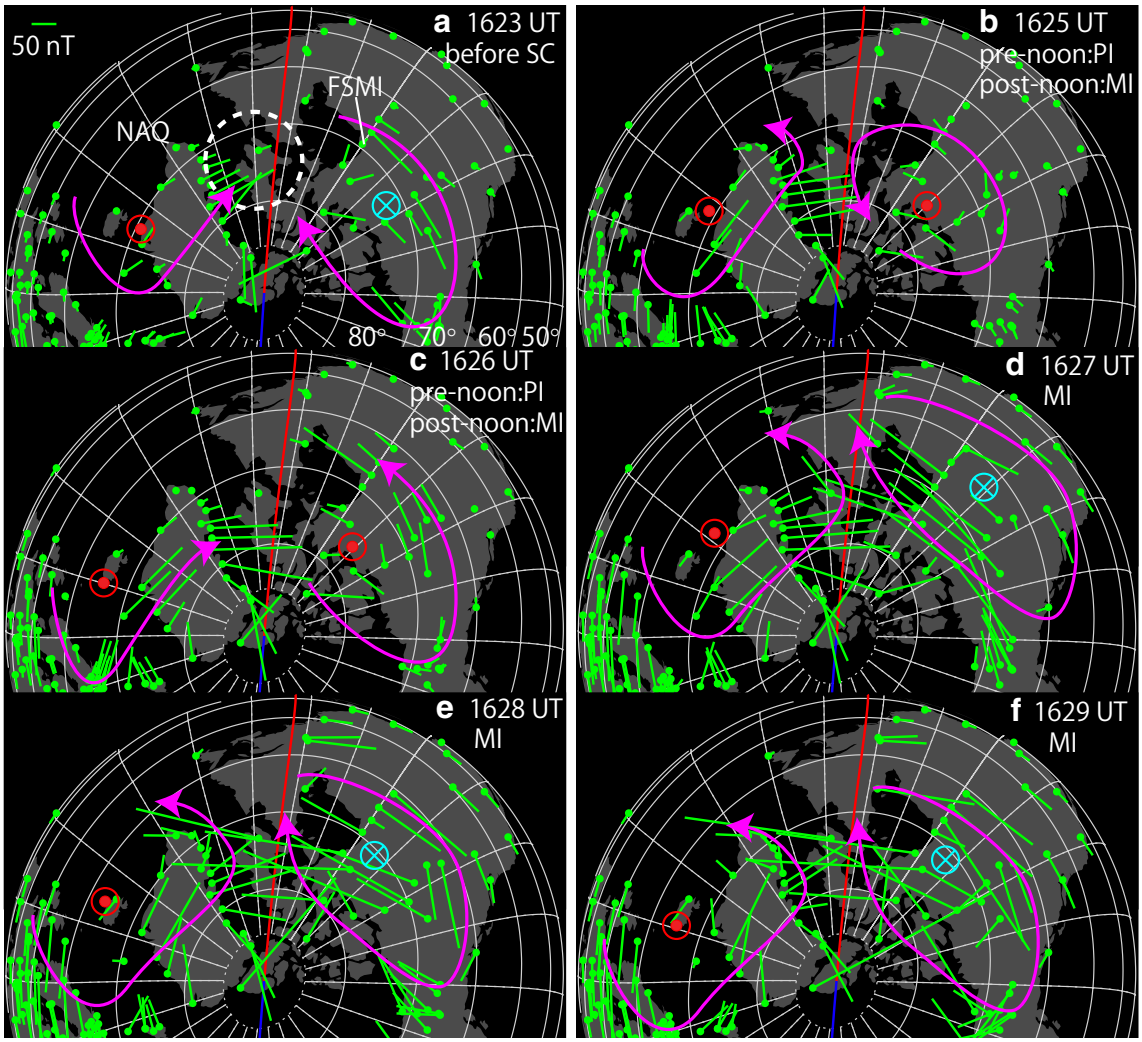

Fig. 9 Same as Fig. 3 but for the May 30, 2003, SC event with 1610 UT as the baseline of **a**

over a 3-h MLT distance across the dawn–dusk meridian. An MI current pair also formed at about the same location at which the PI currents initiated, propagated antisunward, and then became the post-SC DP-2 currents. The overall current pattern is consistent with the model by Araki (1994), and the coexisting current patterns of the PI and MI as well as their antisunward propagation are quite analogous to results from MHD simulations (e.g., Fujita et al. 2003; Samsonov et al. 2010). However, the onsets of the PI and MI were not always simultaneous or symmetric in the pre- and post-noon sectors. The duration and antisunward propagation distance of the PI equivalent currents were also asymmetric in the pre- and post-noon sectors.

By comparing the equivalent currents with the aurora, we identified auroral features that correspond to FACs of the PI and MI current systems, and the high spatial resolution and multiwavelength measurements by imaging can provide more details of the SC-related current evolution. The PI currents can be identified as diffuse auroral brightening that occurs several degrees equatorward of the preexisting discrete aurora (preexisting DP-2 currents). The MI currents can be characterized by the subsequent discrete auroral brightening poleward of the diffuse aurora. Although the overall auroral evolution is consistent with Motoba et al. (2009), we found an interesting dependence on the IMF and PI. When the IMF B_z is negative, discrete auroral brightening occurs equatorward of the preexisting discrete aurora, indicating that the MI currents are located equatorward of the preexisting DP-2. For a positive IMF B_z, the discrete auroral latitude is essentially unchanged with less

Table 1 Normal angle of the interplanetary shocks analyzed in this study

Event	Shock arrival UT at ACE	Shock arrival UT at WIND	Solar wind speed (km/s)	SYM-H rise time (min)	Time lag	MVA			Coplanarity	
					Shock normal angle (X–Y) (deg)	Shock normal angle (X-Y) (deg)	Shock normal angle (XY-Z) (deg)	Med/min eigenvalue ratio	Shock normal angle (X-Y) (deg)	Shock normal angle (XY-Z) (deg)
1 (June 14, 2005)	17:53:57	17:55:42	500	5	176	186	23	2.95	191	36
2 (July 07, 2012)	17:26:30	17:39:00	520	4	192	189	23	2.98	230	74
3 (April 26, 2004)	15:17:36	16:13:30	520	6	173	169	27	10.15	174	−14
4 (May 30, 2003)	15:55:13	15:52:49	750	2	194	211	3	2.90	155	−64

The event number, the shock arrival UT at ACE and WIND, the solar wind speed behind the shock, the SYM-H rise time, and the normal angles in the azimuthal (X-Y) and longitudinal (XY-Z) planes in the three methods are listed. The azimuthal and longitudinal angles are measured from the GSM +X axis toward the +Y axis and from the GSM +Z axis. The satellite locations are shown in Additional file 1: Figure S1, Additional file 2: Figure S2 and Additional file 4: Figure S4, Additional file 5: Figure S5

antisunward propagation; hence, the MI currents appear as a rebrightening of the preexisting DP-2. Although the limited spatial resolution of the magnetometers does not always show the relative locations of these currents, the ground-based auroral imaging clearly separates the evolution of these currents. The difference in the dynamic pressure may also play a role. In addition, the PI current cells propagated antisunward by ~3-h MLT for the negative IMF B_z (event 1), whereas the propagation during the PI cells for a positive IMF B_z was smaller (event 3), indicating that the IMF polarity is important for determining the evolution of the equivalent current pattern.

In events 2 and 4, the PI currents were highly asymmetric with respect to the noon–midnight meridian, and no indication of a post-noon PI was detected within the available magnetometer network. The 557.7-nm diffuse aurora during the PI was much weaker than in the other events, and the lack of a post-noon PI is not because the PI signal was masked by other currents but was indeed substantially weaker than those in the other events with a post-noon PI. The PI in the equatorial magnetometer data of these events was also small or not detected, indicating that the penetration of the electric fields to lower latitudes was also weak. In these events, we found that the interplanetary shock normals were more tilted from the Sun–Earth line than those in the other events. Because PI currents are considered to arise from compressional waves in the equatorial magnetosphere that are convert into Alfven waves propagating into the ionosphere (Fujita et al. 2003), a gradual compression of the magnetosphere would lead to a much weaker PI signal. Since the magnetosphere was compressed from the post-noon side, the post-noon MI started earlier than the pre-noon MI; thus, the PI currents were only seen in the pre-noon sector. The post-noon PI would have arrived substantially later than the MI initiation or far from noon where the ionospheric conductance is much lower. The asymmetric nature of the magnetic field disturbance is analogous to that of the TCVs associated with IMF discontinuities (Zesta and Sibeck 2004), and our interpretation of the shock angle effects is consistent with their idea of the discontinuity angle. Although the IMF B_y generally contributes to the dawn–dusk asymmetry and may be the reason for the asymmetric MI of event 1, it is not likely the cause of the asymmetric PI responses because the IMF $|B_y|$ is large in events 1–3 but the PI asymmetry is seen in events 2 and 4. The Alfvén Mach number is known to alter the SC responses (Yu and Ridley 2011), but the numbers in events 1–3 are in the same range (7–8) and thus do not explain the PI asymmetry.

Liu et al. (2011) inferred that fading of a discrete aurora in the post-noon sector corresponds to the PI phase. None of our events showed such a fading during the PI, but intensification of a diffuse aurora was identified without involving discrete auroral changes. Because their auroral keogram shows a similar fading even before the SC, we think that the fading is due to other dynamic processes of DP-2 currents unrelated to the SC and that PI currents occur equatorward of preexisting DP-2 (discrete aurora) well within closed magnetic field lines. Boudouridis et al. (2003) showed that the polar cap shrinks after shocks. Although we did not see such poleward expansions within our imager FOV, this could be because we focused on several minutes around the SC onset times, whereas they were concerned with changes over longer time scales.

The present study compared an aurora in the dark hemisphere and the magnetic fields in the sunlit hemisphere by taking advantage of the measurements in each hemisphere. The consistency of the initiation times of the PI and MI signals around the conjugate points suggests that the interhemispheric comparison is reasonable. It should be noted, however, that ground magnetic field responses to SCs in the two hemispheres are not the

same. The PI magnitude is larger in the sunlit hemisphere (Sastri et al. 2008), and the current pattern may be different (Kim et al. 2013). Although the present study does not compare the current distribution or intensity in the two hemispheres, the auroral brightening locations and intensity in the sunlit hemisphere could be different from the measurements in the dark hemisphere.

Through an analysis of these events, we demonstrated that the combination of magnetometers and an aurora can reveal the detailed evolution of the currents associated with solar wind dynamic pressure pulses and their dependence on the IMF polarity and shock orientation. This approach could be used for other types of solar wind disturbances for understanding the responses of current systems in the magnetosphere–ionosphere coupling system. However, since our results are limited to a case study basis, further examination is needed to evaluate how common the measured signatures are.

Additional files

Additional file 1: Figure S1. (Left) solar wind magnetic field, density, velocity, and dynamic pressure from ACE and WIND, (middle) post-noon magnetometer, and (right) pre-noon magnetometer data during the June 14, 2005, event. Magnetometers are ordered from high to low latitudes.

Additional file 2: Figure S2. Same as Additional file 1 but for the July 14, 2012, event.

Additional file 3: Figure S3. ΔB (vectors) and calculated FACs (blue–red contours) in the AMPERE data at three times for the July 14, 2012, event.

Additional file 4: Figure S4. Same as Additional file 1 but for the April 26, 2004, event.

Additional file 5: Figure S5. Same as Additional file 1 but for the May 30, 2003, event.

Authors' contributions

YN carried out the work and consulted with the other coauthors. All authors read and approved the final manuscript.

Author details

[1] Department of Atmospheric and Oceanic Sciences, University of California, Los Angeles, CA, USA. [2] Solar-Terrestrial Environment Laboratory, Nagoya University, Nagoya, Japan. [3] Research Institute for Sustainable Humanosphere, Kyoto University, Uji, Japan. [4] Department of Earth and Planetary Science, Kyushu University, Fukuoka, Japan. [5] Earthquake Research Institute, University of Tokyo, Tokyo, Japan.

Acknowledgements

This work was supported by NASA Grants NNX13AI61G, NNX15AI62G, and NAS5-02099 and NSF Grants PLR-1341359, AGS-1451911, and AFOSR FA9550-15-1-0179. The South Pole imager has been supported by a cooperative agreement between NSF and the National Institute of Polar Research, Japan. THEMIS, SuperMAG, and MAGDAS/CPMN data were obtained from http://themis.ssl.berkeley.edu as daily CDF files, from http://supermag.jhuapl.edu/ as daily ASCII files, and by A. Yoshikawa (http://magdas.serc.kyushu-u.ac.jp/) as daily ASCII files, respectively, and we thank the individual magnetometer projects for making these data available for this study, including the National Space Institute at the Technical University of Denmark for Greenland magnetometer data. SYM-H, ACE, and WIND data were downloaded as CDF files through http://cdaweb.gsfc.nasa.gov. Contact the authors for the South Pole imager and satellite data used in this study.

Competing interests

The authors declare that they have no competing interests.

Received: 4 April 2016 Accepted: 28 July 2016
Published online: 11 August 2016

References

Araki T (1977) Global structure of geomagnetic sudden commencements. Planet Space Sci 25:373–384. doi:10.1016/0032-0633(77)90053-8

Araki T (1994) A physical model of geomagnetic sudden commencement. In: Engebretson MJ, Takahashi K, Scholer M (eds) Solar wind sources of magnetospheric ultra-low-frequency waves. Geophysical monograph series, vol 81. AGU, Washington, DC, pp 183–200. doi:10.1029/GM081p0183

Araki T, Allen JH, Araki Y (1985) Extension of a polar ionospheric current to the nightside equator. Planet Space Sci 33:11–16

Araki T, Takeuchi T, Araki Y (2004) Rise time of geomagnetic sudden commencements—statistical analysis of ground geomagnetic data—. Earth Planets Space 56:289–293

Boudouridis A, Zesta E, Lyons R, Anderson PC, Lummerzheim D (2003) Effect of solar wind pressure pulses on the size and strength of the auroral oval. J Geophys Res 108:8012. doi:10.1029/2002JA009373

Boudouridis A, Lyons LR, Zesta E, Weygand JM, Ribeiro AJ, Ruohoniemi JM (2011) Statistical study of the effect of solar wind dynamic pressure fronts on the dayside and nightside ionospheric convection. J Geophys Res 116:A10233. doi:10.1029/2011JA016582

Chi PJ et al (2001) Propagation of the preliminary reverse impulse of sudden commencements to low latitudes. J Geophys Res 106(A9):18857–18864. doi:10.1029/2001JA900071

Ebihara Y, Tanaka Y-M, Takasaki S, Weatherwax AT, Taguchi M (2007) Quasi-stationary auroral patches observed at the South Pole Station. J Geophys Res 112:A01201. doi:10.1029/2006JA012087

Egeland A, Burke WJ, Maynard NC, Basinska EM, Winningham JD, Deehr CS (1994) Ground and satellite observations of postdawn aurorae near the time of a sudden storm commencement. J Geophys Res 99(A2):2095–2108. doi:10.1029/92JA03027

Engebretson MJ et al (1999) A multipoint determination of the propagation velocity of a sudden commencement across the polar ionosphere. J Geophys Res 104(A10):22433–22451. doi:10.1029/1999JA900237

Fujita S, Tanaka T, Kikuchi T, Fujimoto K, Hosokawa K, Itonaga M (2003) A numerical simulation of the geomagnetic sudden commencement: 1. Generation of the field-aligned current associated with the preliminary impulse. J Geophys Res 108:1416. doi:10.1029/2002JA009407

Gjerloev JW (2012) The SuperMAG data processing technique. J Geophys Res 117:A09213. doi:10.1029/2012JA017683

Han D-S, Yang H-G, Liang J, Iyemori T, Cowley SWH, Araki T (2010) High-latitude reconnection effect observed at the dayside dip equator as a precursor of a sudden impulse. J Geophys Res 115:A08214. doi:10.1029/2009JA014787

Hardy DA, Schmitt LK, Gussenhoven MS, Marshall FJ, Yeh HC, Schumaker TL, Huber A, Pantazis J (1984) Precipitating electron and ion detectors (SSJ/4) for the block 5D/Flights 6–10 DMSP satellites: calibration and data presentation. Rep. AFGL-TR-84-0317 Air Force Geophysics Laboratory, Hanscom AFB, Mass. http://www.dtic.mil/dtic/tr/fulltext/u2/a157080.pdf

Holmes JM, Johnsen MG, Deehr CS, Zhou X-Y, Lorentzen DA (2014) Circumpolar ground-based optical measurements of proton and electron shock aurora. J Geophys Res Space Phys 119:3895–3914. doi:10.1002/2013JA019574

Keika K et al (2009) Deformation and evolution of solar wind discontinuities through their interactions with the Earth's bow shock. J Geophys Res 114:A00C26. doi:10.1029/2008JA013481

Kikuchi T (1986) Evidence of transmission of polar electric fields to the low latitude at times of geomagnetic sudden commencements. J Geophys Res 91:3101–3105. doi:10.1029/JA091iA03p03101

Kikuchi T (2014) Transmission line model for the near-instantaneous transmission of the ionospheric electric field and currents to the equator. J Geophys Res Space Phys 119:1131–1156. doi:10.1002/2013JA019515

Kikuchi T, Tsunomura S, Hashimoto K, Nozaki K (2001) Field-aligned current effects on midlatitude geomagnetic sudden commencements. J Geophys Res 106(A8):15555–15565. doi:10.1029/2001JA900030
Kim K-H, Park KS, Ogino T, Lee D-H, Sung S-K, Kwak Y-S (2009) Global MHD simulation of the geomagnetic sudden commencement on 21 October 1999. J Geophys Res 114:A08212. doi:10.1029/2009JA014109
Kim H, Cai X, Clauer CR, Kunduri BSR, Matzka J, Stolle C, Weimer DR (2013) Geomagnetic response to solar wind dynamic pressure impulse events at high-latitude conjugate points. J Geophys Res Space Phys 118:6055–6071. doi:10.1002/jgra.50555
Liou K, Newell PT, Shue J-H, Meng C-I, Miyashita Y, Kojima H, Matsumoto H (2007) "Compression aurora": particle precipitation driven by long-duration high solar wind ram pressure. J Geophys Res 112:A11216. doi:10.1029/2007JA012443
Liu JJ, Hu HQ, Han DS, Araki T, Hu ZJ, Zhang QH, Yang HG, Sato N, Yukimatu AS, Ebihara Y (2011) Decrease of auroral intensity associated with reversal of plasma convection in response to an interplanetary shock as observed over Zhongshan station in Antarctica. J Geophys Res 116:A03210. doi:10.1029/2010JA016156
Meurant M, Gérard J-C, Blockx C, Hubert B, Coumans V (2004) Propagation of electron and proton shock-induced aurora and the role of the interplanetary magnetic field and solar wind. J Geophys Res 109:A10210. doi:10.1029/2004JA010453
Motoba T, Kadokura A, Ebihara Y, Frey HU, Weatherwax AT, Sato N (2009) Simultaneous ground-satellite optical observations of postnoon shock aurora in the Southern Hemisphere. J Geophys Res 114:A07209. doi:10.1029/2008JA014007
Nishida A (1964) Ionospheric screening effect and storm sudden commencement. J Geophys Res 69(9):1861–1874. doi:10.1029/JZ069i009p01861
Nishimura Y et al (2013) Structures of dayside whistler-mode waves deduced from conjugate diffuse aurora. J Geophys Res Space Phys 118:664–673. doi:10.1029/2012JA018242
Peng Z, Wang C, Hu YQ, Kan JR, Yang YF (2011) Simulations of observed auroral brightening caused by solar wind dynamic pressure enhancements under different interplanetary magnetic field conditions. J Geophys Res 116:A06217. doi:10.1029/2010JA016318
Rich FJ (1984) Fluxgate magnetometer (SSM) for the Defense Meteorological Satellite Program (DMSP) Block 5D-2, flight 7. Tech. Rep. AFGL-TR-84-0225, Air Force Geophysics Laboratory, Hanscom Air Force Base, Mass. http://www.dtic.mil/dtic/tr/fulltext/u2/a155229.pdf
Richmond AD, Kamide Y (1988) Mapping electrodynamic features of the high-latitude ionosphere from localized observations: technique. J Geophys Res 93(A6):5741–5759. doi:10.1029/JA093iA06p05741
Russell CT, Chi PJ, Dearborn DJ, Ge YS, Kuo-Tiong B, Means JD, Pierce DR, Rowe KM, Snare RC (2008) THEMIS ground-based magnetometers. Space Sci Rev 141:389–412. doi:10.1007/s11214-008-9337-0
Samsonov AA, Sibeck DG, Yu Y (2010) Transient changes in magnetospheric-ionospheric currents caused by the passage of an interplanetary shock: Northward interplanetary magnetic field case. J Geophys Res 115:A05207. doi:10.1029/2009JA014751
Sastri JH, Takeuchi T, Araki T, Yumoto K, Tsunomura S, Tachihara H, Luehr H, Watermann J (2001) Preliminary impulse of the geomagnetic storm sudden commencement of November 18, 1993. J Geophys Res 106(A3):3905–3918. doi:10.1029/2000JA000226
Sastri JH, Yumoto K, Rao JVSV, Ikeda A (2008) Summer-winter hemisphere asymmetry of the preliminary reverse impulse of geomagnetic storm sudden commencements at midlatitudes. J Geophys Res 113:A05302. doi:10.1029/2007JA012968
Shinbori A, Tsuji Y, Kikuchi T, Araki T, Watari S (2009) Magnetic latitude and local time dependence of the amplitude of geomagnetic sudden commencements. J Geophys Res 114:A04217. doi:10.1029/2008JA013871
Slinker SP, Fedder JA, Hughes WJ, Lyon JG (1999) Response of the ionosphere to a density pulse in the solar wind: simulation of traveling convection vortices. Geophys Res Lett 26:3549–3552. doi:10.1029/1999GL010688
Stauning P, Troshichev OA (2008) Polar cap convection and PC index during sudden changes in solar wind dynamic pressure. J Geophys Res 113:A08227. doi:10.1029/2007JA012783
Sun W, Lee LC, Kamide Y, Akasofu S-I (1985) An improvement of the Kamide-Richmond-Matsushita Scheme for the estimation of the three-dimensional current system. J Geophys Res 90(A7):6469–6474. doi:10.1029/JA090iA07p06469
Sun TR, Wang C, Zhang JJ, Pilipenko VA, Wang Y, Wang JY (2015) The chain response of the magnetospheric and ground magnetic field to interplanetary shocks. J Geophys Res Space Phys 120:157–165. doi:10.1002/2014JA020754
Takeuchi T, Russell CT, Araki T (2002) Effect of the orientation of interplanetary shock on the geomagnetic sudden commencement. J Geophys Res 107(A12):1423. doi:10.1029/2002JA009597
Tamao T (1964) A hydromagnetic interpretation of geomagnetic SSC*. Rep Ionos Space Res Jpn 18:16–31
Wang C, Li CX, Huang ZH, Richardson JD (2006) Effect of interplanetary shock strengths and orientations on storm sudden commencement rise times. Geophys Res Lett 33:L14104. doi:10.1029/2006GL025966
Yamada Y, Takeda M, Araki T (1997) Occurrence characteristics of the preliminary impulse of geomagnetic sudden commencement detected at middle and low latitudes. J Geomag Geoelectr 49:1001–1012
Yu Y-Q, Ridley AJ (2011) Understanding the response of the ionosphere-magnetosphere system to sudden solar wind density increases. J Geophys Res 116:A04210. doi:10.1029/2010JA015871
Yumoto K, the MAGDAS Group (2006) MAGDAS project and its application for space weather. In: Gopalswamy N, Bhattacharyya A (eds) Solar influence on the heliosphere and earth's environment: recent progress and prospects. ISBN-81-87099-40-2, pp 309–405
Zesta E, Singer HJ, Lummerzheim D, Russell CT, Lyons LR, Brittnacher MJ (2000) The effect of the January 10, 1997 pressure pulse on the magnetosphere-ionosphere current system. In: S-I Ohtani, Fujii R, Hesse M, Lysak RL (eds) Magnetospheric current systems. American Geophysical Union, Washington, D.C. doi:10.1029/GM118p0217
Zesta E, Sibeck DG (2004) A detailed description of the solar wind triggers of two dayside transients: events of 25 July 1997. J Geophys Res 109:A01201. doi:10.1029/2003JA009864
Zhang Y, Paxton LJ, Zheng Y (2008) Interplanetary shock induced ring current auroras. J Geophys Res 113:A01212. doi:10.1029/2007JA012554
Zhou X-Y, Tsurutani BT (1999) Rapid intensification and propagation of the dayside aurora: large scale interplanetary pressure pulses (fast shocks). Geophys Res Lett 26(8):1097–1100. doi:10.1029/1999GL900173
Zhou X-Y, Strangeway RJ, Anderson PC, Sibeck DG, Tsurutani BT, Haerendel G, Frey HU, Arballo JK (2003) Shock aurora: FAST and DMSP observations. J Geophys Res 108:8019. doi:10.1029/2002JA009701